PERGAMON

Planetary and Space Science 47 (1999) 1409–1422

Planetary and Space Science

Radar observations of comets

J.K. Harmon[a,*], D.B. Campbell[b], S.J. Ostro[c], M.C. Nolan[a]

[a]*Arecibo Observatory, HC3 Box 53995, Arecibo, PR, 00612, USA*
[b]*Astronomy Department, Cornell University, Ithaca, NY, 14853, USA*
[c]*Jet Propulsion Laboratory, California Institute of Technology, Pasadena, CA, 91109-8099, USA*

Received 19 November 1998; accepted 2 February 1999

Abstract

Seven comets have been detected by Earth-based radars during the period 1980–1998. All but one of these gave a detectable echo from the nucleus, while three of the comets also showed a broad-band echo from large (~cm-size) grains in the inner coma. Although all observations have been of the CW (continuous-wave) type, which precludes direct size measurement, the radar cross sections are consistent with nucleus diameters averaging a few kilometers and varying over a range of ten. Comparisons with independent size estimates indicate relatively low radar albedos, implying nucleus surface densities of 0.5 to 1 g/cm^3. The surfaces of comet nuclei appear to be as rough as typical asteroid surfaces, but are considerably less dense. Analysis of coma echoes indicates that some comets emit large grains at rates (~ton/s) which are comparable with their gas and dust production rates. There is also some indirect evidence for grain evaporation or fragmentation within a few hundred to a few thousand kilometers of the nucleus. The highest priority of future radar observations will be to obtain delay-Doppler images of a nucleus, which would give direct size and shape estimates as well as a more reliable albedo. Delay-Doppler or interferometric imaging of the coma echo would also help to better characterize the grain halo. Ten short-period comets are potentially detectable during the next two decades, although the best radar opportunities may well come from comets yet to be discovered.

1. Introduction

Occasionally a comet passes close enough to the Earth to be observable with the powerful planetary radars at Arecibo or Goldstone. The detectable echoes from such a comet can come from the nucleus or from a halo of large grains in the inner coma, or both. One great advantage of radar is that it can probe the nucleus directly with little obscuration or confusion because, unlike the visual coma, the grain coma is optically thin and has its own distinguishing echo signature. The coma echo is also interesting in its own right, as it provides perhaps the most unambiguous measure of the large-grain population, which is now being recognized as an important component of a comet's total mass loss. The major drawback of cometary radar is that few of these small objects pass close enough to be detectable. To date, only seven comet radar detections have been made, of which only three could be considered strong. Good radar opportunities are much more frequent for the comparably-sized near-Earth asteroids (NEAs), because of their larger numbers, which may account for why several NEAs have been successfully delay-Doppler imaged while no comet nucleus has. Clearly, radar imaging of a comet nucleus must be the next major goal of future cometary radar research because of its potential for providing direct measures of a nucleus' size, shape, and rotation.

Despite their shortcomings, past cometary radar observations have produced some interesting and important findings. In this paper we review the results from this 'pre-imaging era' of comet radar and preview the future of the field. We begin with a brief historical review of past observations. This is followed by two

* Corresponding author. Tel.: +1-787-878-2612; fax: +1-787-878-1861.

E-mail address: harmon@naic.edu (J.K. Harmon).

0032-0633/99/$20.00
PII: S0032-0633(99)00068-9

Table 1
Comet radar detections

Comet[a]	Year	Site[b]	λ (cm)	Dist. (AU)	Reference
Encke	1980	A	12.6	0.32	Kamoun et al. (1982b)
GS	1982	A	12.6	0.33	Kamoun (1983)
IAA	1983	G	12.9, 3.5	0.033, 0.072	Goldstein et al. (1984)
		A	12.6	0.033	Harmon et al. (1989)
SSF	1983	A	12.6	0.076	Campbell et al. (1983)
Halley	1985	A	12.6	0.63	Campbell et al. (1989)
Hyakutake	1996	G	3.5	0.10	Harmon et al. (1997)
LINEAR	1998	A	12.6	0.196	This paper.

[a] GS = Grigg–Skjellerup, IAA = IRAS–Araki–Alcock, SSF = Sugano–Saigusa–Fujikawa.
[b] A = Arecibo, G = Goldstone.

sections that discuss, in some detail, the implications of the nucleus echoes and coma echoes, respectively; here more emphasis will be given to comparing the various comets than was the case in previous papers. The final section is devoted to a discussion of future prospects, with an emphasis on delay-Doppler imaging.

2. Review of past observations

A list of radar-detected comets is given in Table 1. All of the detections have been made with either the Arecibo telescope in Puerto Rico or the Goldstone antenna in California, with only one comet (IRAS–Araki–Alcock) having been detected at both sites. Three of these comets (Encke, Grigg–Skjellerup, and Halley) are short-period objects, the remainder being newly-discovered comets with very long periods.

All of the successful comet radar detections were made using the same basic CW (continuous-wave) technique. Here, an unmodulated (effectively monochromatic) wave is transmitted with circular polarization. The echo is then received in both (orthogonal) senses of circular polarization. These receive polarization senses are referred to as the OC sense (for 'opposite circular'; also called the 'polarized' or 'expected' sense) and SC sense (for 'same circular'; also called the 'depolarized' or 'unexpected' sense). The OC echo is the stronger of the two for most planetary targets, being the expected sense for specular reflection, whereas the SC echo is normally attributed to depolarization by wavelength-scale roughness. The standard data reduction involves calculation of the frequency spectrum of the received signal to isolate the Doppler-broadened echo in each polarization. In the case of the nucleus echo, this Doppler broadening is associated with the apparent rotation of the nucleus as seen from Earth. The nucleus echo, if detectable, shows up as a relatively narrow (few-Hz-wide) feature sticking up above a flat background noise pedestal. Fig. 1 shows examples of nucleus spectra for the cases of high, moderate, and low signal-to-noise ratio. After subtracting a noise baseline, the echo power is integrated across the nucleus spectrum to estimate the radar cross section σ^{nucl}. In Table 2 we list the nucleus OC cross section $\sigma_{\mathrm{oc}}^{\mathrm{nucl}}$ as well as the circular polarization ratio $\mu_{\mathrm{c}}^{\mathrm{nucl}} = \sigma_{\mathrm{sc}}^{\mathrm{nucl}}/\sigma_{\mathrm{oc}}^{\mathrm{nucl}}$.

Following several failed attempts on various comets during the 1970's (see Kamoun et al., 1982a, for some history), a weak detection was finally made of Comet P/Encke using the Arecibo radar in 1980 (Kamoun et al., 1982b). The radar cross section (Table 2) and narrow bandwidth of the echo were consistent with reflection off a solid nucleus with a diameter ranging from a kilometer to several kilometres. This was followed less than two years later by the detection of Comet P/Grigg–Skjellerup at Arecibo (Kamoun, 1983). This comet was observed when it was at the same distance as Encke (0.33 AU), and, like Encke, gave a weak, narrow-band echo from its nucleus. Although the Grigg–Skjellerup observation was the first to use dual-polarization reception (the Encke observation used OC only), an SC echo was not detected. The OC radar cross section of this comet was 0.5 km^2, suggesting a nucleus perhaps a bit smaller than Encke's.

On 11 May 1983, Comet IRAS–Araki–Alcock (C/1983 H1; henceforth abbreviated IAA) passed within

Table 2
Comet radar parameters

Comet	λ (cm)	$\sigma_{\mathrm{oc}}^{\mathrm{nucl}}$ (km^2)	$\mu_{\mathrm{c}}^{\mathrm{nucl}}$	$\sigma_{\mathrm{oc}}^{\mathrm{coma}}$ (km^2)	$\mu_{\mathrm{c}}^{\mathrm{coma}}$
Encke	12.6	1.1 ± 0.7			
GS	12.6	0.5 ± 0.13	< 0.3		
IAA	12.6	2.14 ± 0.4	0.105 ± 0.005	0.80 ± 0.16	0.014 ± 0.003
	12.9	2.25		0.8	
	3.5	4.44	0.25		
SSF	12.6	0.034 ± 0.008	0.23 ± 0.03		
Halley	12.6	< 3.5		32 ± 10	0.52 ± 0.26
Hyakutake	3.5	0.13 ± 0.03	0.49 ± 0.10	1.33 ± 0.28	0.31 ± 0.12
LINEAR	12.6	0.031 ± 0.015	< 0.5		

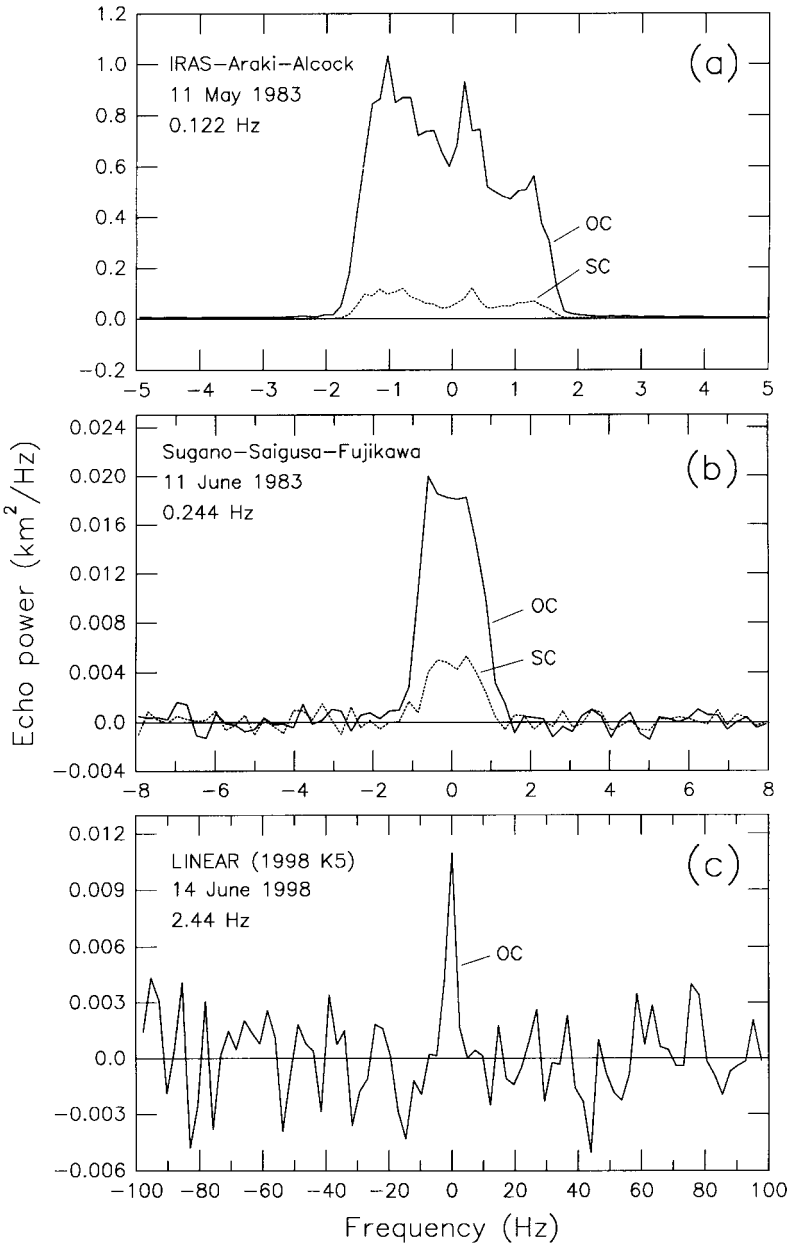

Fig. 1. Doppler spectra of the nucleus echoes for comets (a) IRAS–Araki–Alcock, (b) Sugano–Saigusa–Fujikawa, and (c) LINEAR. Shown are the OC (solid line) and SC (dotted line) polarization components. The frequency resolution (in Hz) is given for each plot.

0.031 AU of the Earth, the closest comet approach since that of Comet Lexell (0.015 AU) in 1770. Very strong echoes were detected on 11 May with the Arecibo and Goldstone S-band (wavelength $\lambda = 13$ cm) radars, and again on 14 May with the Goldstone X-band ($\lambda = 3.5$ cm) radar (Goldstein et al., 1984; Harmon et al., 1989). Thanks to the high echo strength, this was the first comet nucleus echo to give a well-resolved Doppler spectrum, as well as the first to be detected in the SC polarization (Fig. 1(a)). IAA was also the first comet to show a broad-band echo from large coma grains in addition to the expected narrow-band nucleus echo (Fig. 2(a)). The Arecibo and Goldstone S-band cross sections for IAA (which were measured on May 11.9 UT) were in good agreement, giving values of $\sigma_{oc}^{nucl} \approx 2.2$ km^2 and $\sigma_{oc}^{coma} = 0.8$ km^2 for the nucleus and coma components, respectively (Table 2). The fact that the Goldstone X-band observation of May 14.1 UT gave a nucleus cross section twice the S-band value (Table 2) has been attributed to the oblong nucleus showing a larger projected area at the later epoch (Sekanina, 1988), although some intrinsic wavelength dependence cannot be ruled out. One very interesting result from the Arecibo observations was the measurement of extremely low (~1%) depolarization for the coma echo (see

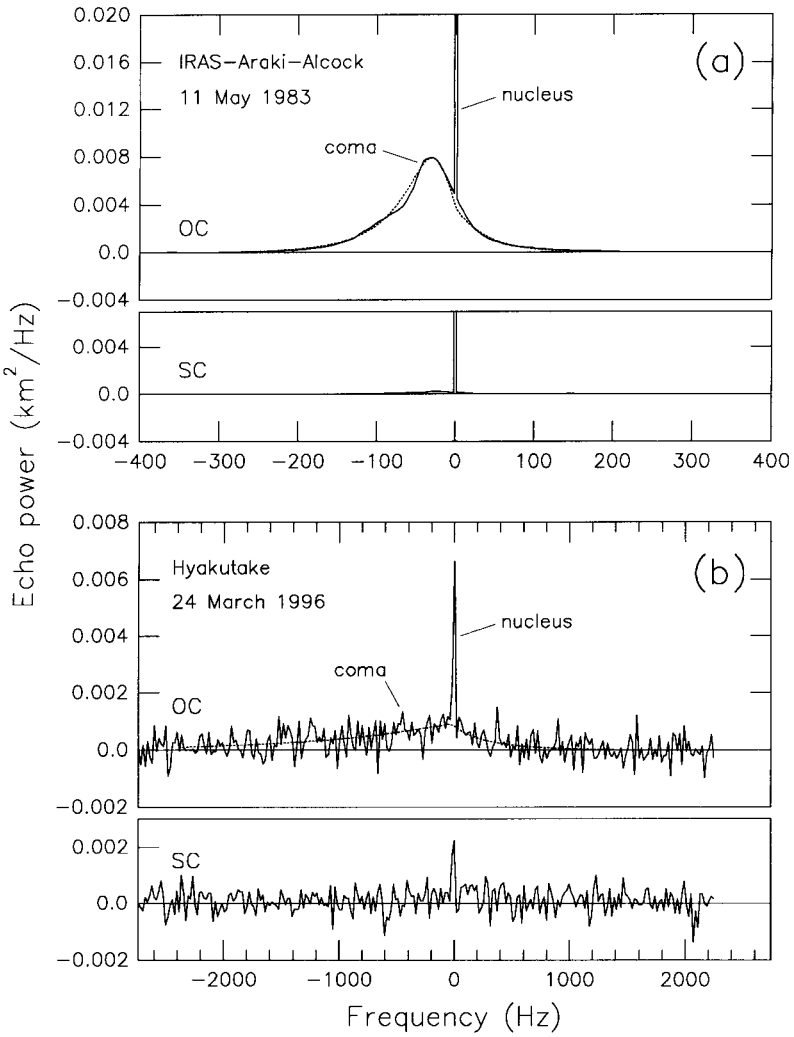

Fig. 2. Doppler spectra (OC and SC polarizations) of the full echo (nucleus and coma components) for comets (a) IRAS–Araki–Alcock, and (b) Hyakutake. The IAA nucleus echo has been truncated at about 2% of its maximum amplitude. The coma component of the IAA echo has been smoothed to 10-Hz resolution from its raw resolution of 0.122 Hz. The Hyakutake spectra have 19.5-Hz resolution. Overplotted on the data are model spectra for the coma echo (dotted curves). The Hyakutake figure is reprinted with permission from Science (vol. 278, p. 1922). Copyright 1997 American Association for the Advancement of Science.

Table 2 and Fig. 2(a)), the lowest ever measured for a solar system target.

In a remarkable coincidence, another close approach occurred only one month after that of IAA, when Comet Sugano–Saigusa–Fujikawa (C/1983 J1; henceforth abbreviated SSF) came within 0.063 AU. Arecibo observations of SSF yielded nucleus detections in both polarizations on three successive days (Campbell et al., 1983). Fig 1(b) shows the echo from 11 June 1983, when SSF's distance was 0.076 AU. The echo was much weaker than that of IAA, due to its greater distance and extremely low radar cross section. With a σ^{nucl} of only 0.04 km^2 (Table 2), this must have been a very small object.

The year 1985 saw the long-awaited return of Comet Halley, and another attempt at a comet radar detection from Arecibo. Unfortunately, Halley was at an unfavorably large distance (0.63 AU) when it was observed at Arecibo on its inbound passage in late November and early December of that year. (It was outside the telescope's declination window during its closer outbound pass in April 1986.) Nevertheless, a weak echo was detected that gave the highest radar cross section (32 km^2) for any comet to date (Campbell et al., 1989). The cross section and large (100 Hz) bandwidth indicated that this was a coma-grain echo similar to that from IAA. No echo was detected from Halley's nucleus, although an upper limit to the nucleus cross section was estimated which was consistent with the size determined from the Giotto spacecraft images.

After Halley came a long dry spell for cometary radar. Arecibo and Goldstone observed the 0.25 AU passage of Comet Austin (1989c$_1$) in May 1990, but,

despite tantalizing hints of echoes at both sites, no clear detection could be reported. A brief, unsuccessful attempt on the short-period comet P/Honda–Mrkos–Pajdusakova was made at Goldstone when it came within 0.25 AU a few months later.

The drought was finally broken in 1996 with the appearance of the new comet Hyakutake (C/1996 B2), the first visually spectacular comet to make a close approach (0.10 AU) since Halley in 1910. Although the Arecibo radar was unavailable due to telescope upgrading, a Hyakutake detection was obtained with the Goldstone X-band radar (Ostro, 1996; Harmon et al., 1997). This comet showed echoes from both nucleus and coma grains (Fig. 2(b)), making it only the second comet to do so. Another brilliant comet, Hale–Bopp (C/1995 O1), followed close on the heels of Hyakutake, but this comet's large distance would have made it a poor radar target for Arecibo even had the upgraded telescope been ready in time. Goldstone observations of Hale–Bopp in April 1997 at a distance of 1.3 AU produced an uninteresting upper limit for the radar cross section of $60\sqrt{B}$ km^2, where B is the echo's bandwidth in Hz. The upgraded Arecibo radar came on line in the spring of 1998, and one of the first observations with this new system was of Comet LINEAR (C/1998 K5). This visually insignificant comet yielded a weak nucleus detection (Fig. 1(c)) with, not surprisingly, a very low σ^{nucl} comparable to that of SSF (Table 2). This latest detection, though hardly exciting, was an early demonstration of an observation that could not have been made without the enhanced capability afforded by the Arecibo upgrade.

3. Results for the nucleus

The shape and polarization of the nucleus echo spectrum provide some information on the angular scattering characteristics of the nucleus and, hence, on its surface roughness. The strength of the echo, expressed as a radar cross section, can be used to estimate the radar albedo provided one has an independent estimate of the nucleus size. This albedo can be used to estimate the dielectric constant and density of the surface.

3.1. Echo spectrum, polarization, and surface roughness

The nucleus echoes from Comets IAA and SSF (Fig. 1(a) and (b)) indicate that the OC and SC spectra are similar in shape, with a half-power bandwidth (B_{HP}) that is a large fraction of the total (limb-to-limb) bandwidth (B). This is very different from terrestrial planet spectra, which typically have a two-component structure consisting of a narrow ($B_{\mathrm{HP}} \ll B$) OC peak (attributed to quasispecular reflection off large, gentle surface undulations) superimposed on a broad, partially depolarized diffuse echo (attributed to scattering off wavelength-scale structure such as rocks). Apparently, comet radar echoes are dominated by high-angle scattering from very rugged surface relief. The polarization ratios indicate that the effective scale of this relief varies from comet to comet. Comet IAA shows a low μ_{c} indicative of highly specular roughness on scales of meters, whereas Comet SSF shows a higher μ_{c} suggesting some contribution from decimeter-scale roughness that scatters more diffractively. There is also some evidence for a wavelength dependence in the polarization, with IAA showing an X-band μ_{c} which is twice that of its S-band value and with the Hyakutake X-band echo showing the highest μ_{c} yet seen for a comet (Table 2). This suggests there is an extra component of roughness or rubble at pebble scales that gets smoothed over at the S-band wavelength.

In their spectrum shape and polarization, comet nucleus echoes bear a strong resemblance to asteroid echoes. The range of comet polarization ratios ($\mu_{\mathrm{c}}^{\mathrm{nucl}} = 0.1$ to 0.5; Table 2) is similar to that for NEAs (Ostro et al., 1991) and overlaps the 0.05 to 0.2 range for main-belt asteroids or MBAs (Ostro et al., 1985, 1991). The spectrum shapes for comet nuclei (Fig. 1) are also similar to those seen for both NEAs and MBAs. Apparently comets are similar to asteroids in the ruggedness and scale of their surface relief. However, little effort has been made to quantify comet roughness due to lack of suitable theories to deal with this particular scattering regime as well as to limitations in the data themselves. (This contrasts with the situation for terrestrial planet quasispecular echoes, from which rms slope and Fresnel reflectivity estimates are routinely extracted using reasonably well-motivated physical optics theories.) Some attempts have been made to fit the IAA spectrum with the model spectrum,

$$S(f) \propto [1 - (2f/B)^2]^{n/2} \tag{1}$$

which corresponds to the echo spectral shape for a sphere with a scattering law of the form

$$\sigma^0(\theta) \propto \cos^n \theta, \tag{2}$$

where $\sigma^0(\theta)$ is the specific cross section as a function of incidence angle θ. Such 'cosine-law' models are often applied to asteroid echoes and the diffuse-component echoes from terrestrial planets. Harmon et al. (1989) suggested an $n \leq 1$ scattering law for IAA based on the sharp edges of the Arecibo IAA spectrum, and argued that this was evidence for scattering from a chaotic surface with super-wavelength-scale roughness elements giving both specular reflection and shadowing. However, over-interpretation can be a

Table 3
Nucleus: diameter and radar albedo estimates

Comet	Diameter (km)	Method[a]	Albedo[b]
Encke	4.4–9.8	I[c]	0.017–0.083
	< 3.0	M[d]	> 0.16
IAA	8.8	R[e], I[f], C[g]	0.039
SSF	0.74	I[h]	0.098
Halley	10	S[i]	< 0.05
Hyakutake	4.2–4.8	I[j]	0.011–0.015
	< 5.0–6.0	C[k]	> 0.007–0.010
	2.5		0.039 (assumed)
LINEAR	1.1		0.039 (assumed)

[a] Method used to derive the tabulated diameter estimate: I = infrared, R = radar + visual rotation, C = radio continuum, S = spacecraft imaging, M = non-gravitational motion.
[b] Total (OC + SC) radar cross section divided by the projected area $\pi D^2/4$, where D is the tabulated diameter; for OC-only detections (Encke, LINEAR) a 15% SC component has been assumed.
[c] Luu and Jewitt (1990).
[d] Whipple and Sekanina (1979).
[e] Sekanina (1988).
[f] Hanner et al. (1985).
[g] Altenhoff et al. (1983).
[h] Hanner et al. (1987).
[i] Keller et al. (1986).
[j] Sarmecanic et al. (1997), Fernandez et al. (1996).
[k] de Pater et al. (1997), Altenhoff et al. (1996), Jewitt and Matthews (1997), Fernandez et al. (1997).

danger here, as the spectrum shape is influenced not only by the angular scattering law but also by the large-scale shape and irregularity of the nucleus and the particular viewing geometry. For example, Comet SSF observations gave cosine-law fits with n varying between 1.4 and 2.8 over three consecutive days (the spectrum shown in Fig. 1(b) giving the $n = 1.4$ value), and the Goldstone X-band spectrum for Comet IAA showed a highly skewed spectrum on 14 May that differed markedly from the 11 May spectrum (Goldstein et al., 1984). Nevertheless, one can say that comet nucleus echoes are similar to many asteroid echoes in having broad ($B_{HP} \sim B$) spectra corresponding to cosine-law exponents of roughly Lambert-law ($n = 2$) or perhaps smaller. Although the cosine-law was originally interpreted as the monostatic case of a more general bistatic scattering law, more recent radar studies (e.g., Mitchell et al., 1995) have used the cosine law to parameterize a simple geometric optics theory. Here the rms slope θ_r of the surface roughness is related to n by

$$\theta_r = \tan^{-1}\sqrt{2/n}, \quad (3)$$

so that $n = 1$ to 2 cosine scattering laws correspond to $\theta_r \approx 50^\circ$. Apparently there is no avoiding the conclusion that comet nuclei have extremely rough surfaces on meter and larger scales.

3.2. Nucleus size, albedo, and surface density

CW radar observations of comets do not resolve the echo in time delay and, hence, cannot provide a direct measure of nucleus size. The best one can hope to do is to construct a reasonably plausible model specifying the size, shape and spin vector of the nucleus based on multi-day measurements of radar Doppler spectra and visual dust jets/fans. In practice, of course, this is very difficult to do and has only really been attempted for Comet IAA (Sekanina, 1988). Several non-radar methods have been used to estimate sizes of some of the radar-detected comets, and from such independent size estimates one can calculate a radar albedo $\hat{\sigma}$ (the nucleus' radar cross section divided by its projected area). From the radar albedo one can then estimate the dielectric constant and density of the nucleus surface. Also, if the intrinsic spread in radar albedo is not too large, comparisons of the radar cross sections of comet nuclei can provide at least a crude measure of their relative sizes. Roughly speaking, the fact that the measured cross sections span two orders of magnitude (Table 2) suggests that the nucleus sizes span a range of about ten.

Table 3 lists the size estimates and corresponding albedos for the radar-detected comet nuclei. Of these, the values for IAA are probably the most reliable. Sekanina's hybrid (radar bandwidth + optical spin vector) model gives a diameter for IAA which is in good agreement with diameters based on infrared and radio-continuum measurements from the same epoch (Sekanina, 1988). Using his estimate of 61 km^2 for the projected area of the nucleus at the time of the S-band observations (which corresponds to the equivalent spherical diameter of 8.8 km listed in Table 3) we get a radar albedo of 0.039 for IAA. The range of infrared estimates of Encke's diameter gives a broad range of albedos straddling the IAA albedo. An earlier upper limit to the Encke diameter (estimated from its non-gravitational motion) may be suspect, as it gives an albedo (0.16) which is outside the infrared range and much higher than any of the other albedo estimates in Table 3. From infrared observations, Hanner et al. (1987) estimated a very small (< 1 km) diameter for the nucleus of Comet SSF, which agrees with this comet's very low radar cross section. Although the estimated albedo of 0.098 for SSF is relatively high, it would be consistent with the suggestion by Hanner et al. (based on an apparently high thermal inertia and unusually low dust production) that the surface compaction of this nucleus is higher than normal. The Halley radar observations did not detect the nucleus but did give an upper limit to the nucleus cross section that, combined with the Giotto value for the nucleus size, gives an upper limit for the radar albedo that is consistent with the IAA albedo; this upper limit also

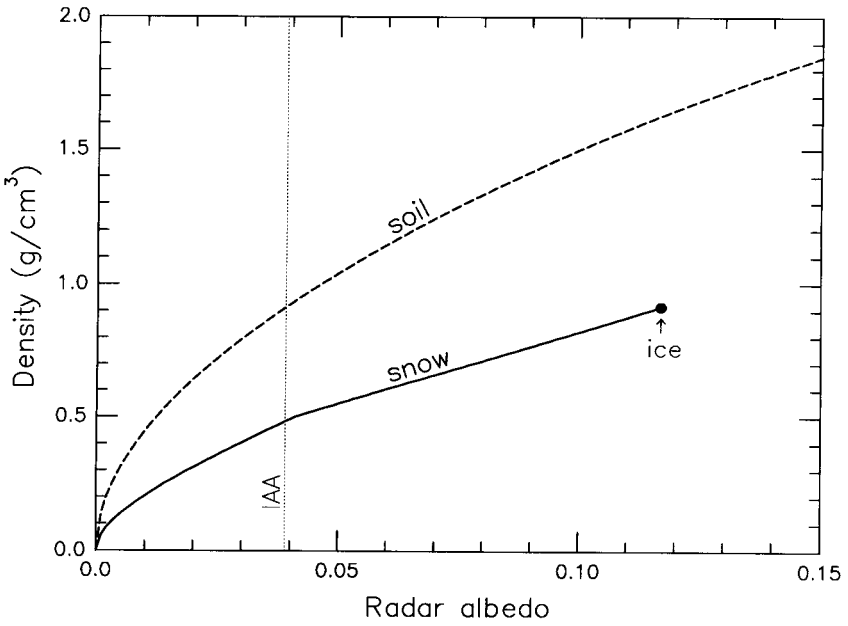

Fig. 3. Bulk density d of the nucleus surface as a function of radar albedo $\hat{\sigma}$ for dry snow (solid curve) and a silicate soil (dashed curve). See text for details. The albedo for Comet IAA is also shown (vertical dotted line).

suggests that the Halley nucleus was on the verge of detectability during the 1985 observations. Using the IAA albedo as a standard, Harmon et al. (1997) estimated Hyakutake's diameter to be 2.5 km, which would make it larger than SSF but much smaller than both Halley and IAA. Infrared observations give a larger (4.5 km) diameter which, if correct, would imply a very low (0.013) radar albedo for this comet. Finally, we estimate the diameter of Comet LINEAR (C/1998 K5) to be about 1 km assuming an IAA-like albedo, placing it in the same size class as Comet SSF. Like SSF, 1998 K5 was a very faint object, with just a hint of a dust tail.

If the nucleus' radar scattering is predominantly specular (as must certainly be the case for a low-μ_c echo such as IAA's), then one has $\rho_0 \approx \hat{\sigma}/g$, where ρ_0 is the Fresnel reflection coefficient at normal incidence and g is the backscatter gain. (Although the OC albedo $\hat{\sigma}_{oc}$ is sometimes used in this context on the grounds that it better represents the specular echo, here we have elected to use the total albedo $\hat{\sigma}$ on the assumption that depolarization extracts power that would otherwise appear in the specular component.) For a $\cos^n \theta$ scattering-law in the geometric optics approximation, one has $g=(n+2)/(n+1)$. The corresponding dielectric constant ϵ is given by

$$\epsilon = \frac{(1+\rho_0^{1/2})^2}{(1-\rho_0^{1/2})^2}. \tag{4}$$

This can then be used to estimate the bulk density d using some suitable expression for $d(\epsilon)$. In Fig. 3 we plot d as a function of $\hat{\sigma}$ for snow and soil surfaces assuming $g = 3/2$ ($n = 1$). Here we have used the expression

$$d \approx \begin{cases} 0.526(\epsilon - 1.00) & (\epsilon \leq 1.95) \\ 0.347(\epsilon - 0.51) & (\epsilon > 1.95) \end{cases} \tag{5}$$

for the case of dry snow (Hallikainen et al., 1986) and

$$d \approx 3.9\left(\frac{\epsilon - 1}{\epsilon + 2}\right) \tag{6}$$

for a soil of silicate powder (Campbell and Ulrichs, 1969). From the figure we see that an IAA-like albedo corresponds to a surface with the consistency of a dense (0.5 g/cm^3) terrestrial snowpack or very fluffy (0.9 g/cm^3) soil. A higher albedo such as that of Comet SSF gives densities closer to that of solid ice or a moderately packed soil. All of the foregoing has assumed that the near surface texture is homogeneous. If the density increases significantly with depth within about a wavelength of the surface, then the graded dielectric interface will tend to give more efficient transmission (hence, less reflection) of the incident radar wave (Simpson, 1976) and such simple $d(\hat{\sigma})$ estimates would underestimate the mean density of the near-surface layers.

A comparison of albedos indicates that the surfaces of comet nuclei are less dense than asteroid surfaces. Most MBAs (Ostro et al., 1985; Magri et al., 1998) and NEAs (Ostro et al., 1991; Benner et al., 1997) have radar albedos in the range 0.1 to 0.2 and average more than three times the albedo of Comet IAA. This should translate directly into a difference in reflectivity ρ_0 (and density), since the similarity between comet

and asteroid scattering implies similar backscatter gains. The relatively low comet surface densities are probably attributable in some way to their icy composition, due either to the lower packing density of snow relative to soils and the absence of bedrock, or to the fluffy texture of a refractory mantle left over by sublimation of surface ices. It is clear, however, that comet radar scattering must be a conventional surface or near-surface scattering process such as that seen for non-ice surfaces, and not the sort of multiple volume scattering that is thought to give rise to the extremely high albedos ($\hat{\sigma} \sim 1$) and inverted polarizations ($\mu_c > 1$) seen in radar echoes from the icy Galilean satellites and polar ice deposits on Mars and Mercury. Comet nucleus ices may be too dirty to support the long subsurface path lengths required for such anomalous ice backscattering. The optical albedo measured for the Halley nucleus by Giotto is extremely low and implies a significant proportion of silicates and possible complex organics which would raise the electrical conductivity (and lossiness) when mixed with surface ices.

4. Results for the grain coma

Modeling the shape and amplitude of the broadband component provides information on properties of coma grains. First, we discuss grain-size constraints from radar cross section and polarization in the context of a simple grain ejection theory. Next, we discuss the extent to which Doppler spectrum modeling can be used to estimate grain ejection velocity/direction and the size of the grain halo. Finally, we treat nucleus mass loss rates inferred from the coma echo strength and compare these with results from other types of observations.

4.1. Grain size constraints and grain ejection

In the Rayleigh approximation ($a < \lambda/2\pi$) a particle of radius a and dielectric constant ϵ has a radar cross section $\sigma = \pi a^2 Q_b(a)$, where the backscatter efficiency Q_b is approximated by

$$Q_b(a) = C_R a^4, \tag{7}$$

and where

$$C_R = 4\left(\frac{2\pi}{\lambda}\right)^4 \left|\frac{\epsilon - 1}{\epsilon + 2}\right|^2. \tag{8}$$

From this it follows that a grain halo with a power-law grain size distribution $n(a) \propto a^{-\alpha}$ and giving a radar cross section σ^{coma} must have a total mass

$$M \approx \sigma^{\text{coma}} \left(\frac{4d}{3C_R}\right)\left(\frac{7-\alpha}{4-\alpha}\right)[1 - (a_0/a_{\max})^{4-\alpha}]a_{\max}^{-3}, \tag{9}$$

where d is the grain density and a_0 and $a_{\max}$ are the minimum and maximum grain sizes in the distribution. Using Eq. (9), Harmon et al. (1989) and Campbell et al. (1989) showed that making $a_{\max} < 0.5$ mm resulted in a total mass in grains exceeding the nucleus mass for both IAA and Halley, from which they concluded that the effective grain size must have been at least a few millimeters. On the other hand, the extremely low depolarization for the IAA coma echo implied $a_{\max} < 5$ cm or so for the grains from that comet (Harmon et al., 1989). Harmon et al. also suggested it was plausible to identify $a_{\max}$ with the gravitational cutoff size a_m in a simple gas-drag theory of dust ejection. Assuming a uniform radial outflow of gas with thermal expansion velocity V_g, this theory has grains ejected with a terminal velocity V_t given by (Harmon et al., 1989, 1997)

$$V_t(a) = C_v a^{-1/2}(1 - a/a_m)^{1/2}, \tag{10}$$

where

$$C_v = \left(\frac{3C_D C_E V_g \dot{\mu} R}{4d}\right)^{1/2} \tag{11}$$

is a velocity scaling factor, and

$$a_m = \frac{9V_g\dot{\mu}}{16\pi G R d_n d} \tag{12}$$

is a maximum grain size in the gravitational correction factor $(1-a/a_m)^{1/2}$. Also, C_D ($=2$ for a sphere) is a drag coefficient, C_E ($\approx 9/4$) corrects for the change in V_g with expansion, $\dot{\mu}$ is the surface gas mass flux, R is nucleus radius, d_n is mean nucleus density, and G is the gravitational constant. Using Eq. (12) it can be shown that an a_m of 5 cm requires a gas flux $\dot{\mu}$ of about 2×10^{-5} g/cm^2-s, which is reasonable given that it is less than the 5×10^{-5} g/cm^2-s sublimation rate for clean ice (at 1 AU) and comparable with the $\dot{\mu}$ required to give the observed total gas production if $\sim$1% of the surface of IAA was actively sublimating (Hanner et al., 1985; Sekanina, 1988).

The apparent cobble-size $a_{\max}$ for IAA grains may not necessarily apply to other comets for which $\dot{\mu}$ may be higher or R smaller. A substantial population of boulder-size and larger chunks would show up in the depolarized echo, since μ_c increases rapidly as $a_{\max}$ exceeds a few times $\lambda/2\pi$ (depending on grain density). This may, in fact, have been the case for both Halley and Hyakutake, which showed some hints of non-negligible SC coma echoes (Table 2). However, for both of these comets the SC coma echo (if real) was very weak compared to the background noise, and future obser-

vations will be needed to confirm the reality of significant coma-echo depolarization for some comets.

Radar is only one of several lines of evidence supporting the important role of large grains in cometary activity. Both comet antitails (Sekanina, 1974) and narrow infrared trails (Eaton et al., 1984) require grains that are confined near the comet orbit, which is best explained by the ejection of large grains at the slow (meters/s) velocities implied by Eq. (10). Also, both the Giotto and Suisei spacecrafts were hit by >mm-size grains during their Halley encounters. Finally, millimeter and submillimeter radio continuum observations are more easily explained if relatively large grains are included in a broad particle size distribution (Jewitt and Luu, 1992).

4.2. Spectrum modeling

Although a grain halo's properties cannot be uniquely characterized from its Doppler spectrum, it is worthwhile to treat the forward problem of comparing the observed spectrum with computed model spectra. One can begin by stating that a spherical grain of radius a will contribute $\pi a^2 Q_b(a)$ to the cross section at a Doppler frequency of

$$f \approx (-2\nu/c)\{\mathbf{v}_{pc} \times \hat{\mathbf{r}}_{ce} + r_{ce}^{-1}[\mathbf{v}_{ce} - (\mathbf{v}_{ce} \cdot \hat{\mathbf{r}}_{ce})\hat{\mathbf{r}}_{ce}] \cdot \mathbf{r}_{pc}\} \quad (13)$$

where ν is the radar frequency, c is the speed of light, $\mathbf{v}_{pc}$ and $\mathbf{r}_{pc}$ are the velocity and distance vectors of the particle relative to the comet, and $\mathbf{v}_{ce}$ and $\hat{\mathbf{r}}_{ce}$ are the velocity vector and distance unit vector of the comet relative to the Earth. One goes from this to a continuous Doppler spectrum $\sigma(f)$ by assuming a continuous particle production size distribution and then summing over discrete emission times and directions, using some appropriate theory to specify the grain ejection. The calculations are relatively easy if one uses a purely radial gas-drag theory (see previous subsection) with negligible radiation pressure, in which case the ejected grains can be treated as free particles moving at velocity V_t [Eq. (10)] in the frame of the nucleus direction vector (Harmon et al., 1989).

Model spectrum fitting along these lines has been done for the coma echoes from IAA (Harmon et al., 1989) and Hyakutake (Harmon et al., 1997), and examples are overplotted on the spectra in Fig. 2(a) and (b). The negative frequency offset of the IAA coma spectrum can be reproduced by invoking a grain emission fan which is oriented roughly sunward, but rotated below the comet orbit plane in a direction consistent with the orientation of the infrared/visual dust emission fan. That the IAA coma spectrum offset could be modeled in this self-consistent way is probably a result of the fact that this comet was a slowly rotating object with an unusually stable sunward fan (Sekanina, 1988). Estimation of the grain velocities is complicated by the fact that the Doppler frequency is determined not only by the grain ejection velocity [the first term within the brackets in Eq. (13)], but also by a spatial component from the varying line-of-sight projection across the radar beam (the second term). Using only the 'velocity term' requires $V_t(1\text{ cm}) = 15$ m/s to give the observed spread in the IAA coma spectrum, whereas including the 'spatial term' for a substantially filled beam lowers this V_t to 8 m/s and gives a better fit to the spectral wings. (In our model this corresponds to $\dot{\mu} = 1.2 \times 10^{-5}$ g/cm^2-s and $a_m = 3.1$ cm, assuming $d_n = 1$ g/cm^3, $R = 5$ km, and $T = 200$ K.) On the other hand, the agreement between the Arecibo and Goldstone σ^{coma} values, despite the three-times-larger Goldstone beam, implies that most of the grains must have been confined to the 2200-km-diameter Arecibo beam. Harmon et al. (1989) suggested that this confinement is evidence for grain evaporation, which is certainly plausible in light of the icy-grain evaporation models of Hanner (1981) and others. An alternative to evaporation would be grain fragmentation (Combi, 1994), which could reduce initially large grains into smaller pieces that backscatter less efficiently.

The grain emission geometry was probably more complicated for Hyakutake, a rapid rotator with an evolving jet structure and antisolar spike. For this and other reasons, Hyakutake was less amenable than IAA to detailed coma echo modeling, although Harmon et al. (1997) could obtain good fits for a plausible range of input parameters [see, for example, the model overplotted in Fig. 2(b)]. Their models suggested that the grain ejection velocities were several times higher than for IAA.

4.3. Grain production rates

If one assumes, as we have here, that the large-grain halo is replenished by continuous particle ejection, then the halo's radar cross section can be used to estimate the mass-loss rate in grains. Although this can be done as part of the spectrum modeling just discussed, it is easier and more instructive to take a simplified analytic approach. Adopting the simple radial outflow model described earlier and assuming that the grains are ejected isotropically with a $\dot{n}(a) \propto a^{-\alpha}$ production-rate size distribution, one can easily derive the following expression for the mass loss rate $\dot{M}$ (Harmon et al., 1989, 1997):

$$\dot{M}(a_m) = \sigma^{coma}\left(\frac{8Rd}{3}\right)\left(\frac{4}{3}\pi G C_D C_E d_n\right)^{1/2}[1 - (a_0/a_m)^{4-\alpha}]a_m^{9/2-\alpha}[(4-\alpha)\pi h I]^{-1} \quad (14)$$

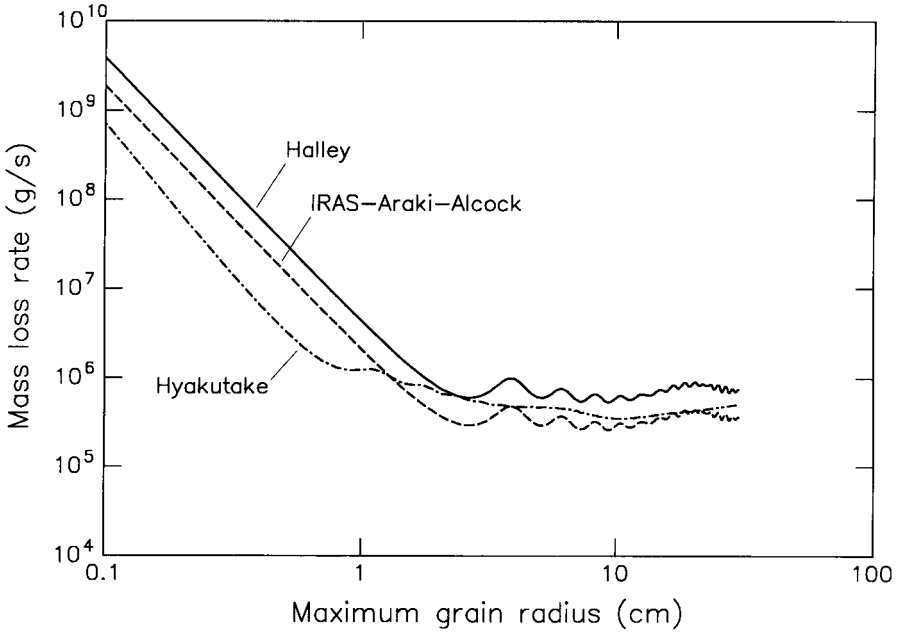

Fig. 4. Radar-derived estimates for the mass loss rate $\dot{M}$ vs maximum grain radius for comets Halley (solid curve), IRAS–Araki–Alcock (dashed curve), and Hyakutake (dot–dashed curve). The grains are assumed to be 0.5 g/cm^3 snowballs with an $a^{-3.5}$ production size distribution.

where

$$I = \int_{a_0}^{a_m} \frac{a^{5/2-\alpha} Q_b(a)}{(1 - a/a_m)^{1/2}}\, da \tag{15}$$

and h is the halfwidth of the cylinder defined by the radar beam at the comet. For $a < \lambda/2\pi$ one gets a Rayleigh approximation for $\dot{M}$ by using the following analytic solution for the integral

$$I = C_R B(1/2,\ 15/2 - \alpha) a_m^{15/2-\alpha} \tag{16}$$

where B is the beta function. Implicit in Eq. (14) is the assumption that the velocity scale factor C_v is a function of a_m. If, on the other hand, one has an independent estimate of C_v (say, from the width of the Doppler spectrum), then one could treat it (and a_m) as a constant, to give the modified expression

$$\dot{M}(a_{max}) = \sigma^{coma}\left(\frac{8C_v d}{3}\right)[1 - (a_0/a_{max})^{4-\alpha}] a_{max}^{4-\alpha} [(4-\alpha)\pi h I]^{-1} \tag{17}$$

where a_{max} ($< a_m$) can be taken as some other (non-gravitational) cutoff size that replaces a_m as the upper integration limit in Eq. (15).

In Fig. 4 we show results of mass-loss rate calculations for the three coma-echo comets. Here we have used Eq. (14) to calculate $\dot{M}(a_m)$ for IAA and Halley, and Eq. (17) to calculate $\dot{M}(a_{max})$ for Hyakutake (assuming $V_t(1\text{ cm}) = 40$ m/s). Mie theory was used to calculate Q_b assuming the grains to be spherical snowballs with density $d = 0.5$ g/cm^3. We took the production rate size distribution to be an $\dot{n}(a) \propto a^{-3.5}$ power-law between $a_0 = 1$ μm and the cutoff size. The $\alpha = 3.5$ power-law was chosen not only because it conforms to size distributions measured for Halley (McDonnell et al., 1986) and Hyakutake (Fulle et al., 1997), but also because it has the convenient property of giving an $\dot{M}$ which is determined primarily by the larger (radar-reflecting) grains and which is relatively insensitive to the precise α. (Steeper size distributions with $\alpha > 4$, such as those commonly used in pre-Halley dust modeling, given an $\dot{M}$ which is dominated by small dust particles and which, when tied at the large-size end by radar measurements, is very sensitive to the precise α assumed.) The Rayleigh regime ($a_m < \lambda/2\pi$) in Fig. 4 shows the $\dot{M}(a_m) \propto a_m^{-3}$ behavior expected from substitution of Eq. (16) in Eq. (14). It is this strong Rayleigh size dependence that requires the presence of large (> mm) grains in order to explain the radar cross sections for reasonable mass-loss rates; for example, taking $a_m = 1$ mm implies an $\dot{M}$ which would have a typical comet nucleus losing most of its mass during a single perihelion passage. The $\dot{M}$ curves flatten out at the larger sizes ($a_m > \lambda/2\pi$), corresponding to large-grain production rates in the range 3×10^5 to 1×10^6 g/s. These rates should be thought of as lower limits for the large grain production, not only because the size cutoff may actually be on the Rayleigh slope, but also because the calculations assume there is no evaporation or fragmentation of the grains during their passage across the beam.

One way to place these grain production rates in some perspective is to compare them with the comets' gas production. The gas production rates for IAA, Halley, and Hyakutake were estimated to be 6×10^5, 5×10^6, and 5×10^6 g/s, respectively, at the times of the radar observations. This implies that the large-grain production rates were, at the very least, only a few times smaller than the gas production rates, and possibly were comparable with them. This is an important result, since it implies that evaporation of large icy grains could be an important source of the gas observed in cometary comae. One can also argue from the gas-rate comparison that the grain cutoff size could not have been much less than 1 cm for these comets, since not only would this imply severe mass-loading of the very gas needed to eject the grains, but also would result in much higher gas production than that observed if the grains were, in fact, evaporating.

One can also compare the large-grain production with dust production. Infrared and visual photometry sensitive to smaller (<30 μm) dust particles gives production rate estimates of $1–2 \times 10^5$, 2×10^6, and 5×10^6 g/s for IAA, Halley, and Hyakutake, respectively, at the times of the radar observations. A straightforward comparison with Fig. 4 would then suggest that (unless $a_m < \lambda/2\pi$) dust production exceeded large-grain production for both Halley and Hyakutake, which is inconsistent with an $\alpha < 4$ power-law distribution. On the other hand, the relative importance of the largest grains to the total particulate mass loss (at ejection) may be underestimated if these grains undergo evaporation or fragmentation while inside the radar beam. In fact, Campbell et al. (1989) suggested grain evaporation to explain why the radar-derived grain production rate for Halley was several times smaller than that deduced from the Giotto spacecraft's particle detectors, a quite plausible explanation given the large (21,000 km) size of the radar beam at Halley. Grain evaporation/fragmentation could also help to resolve the apparent discrepancy between the radar and radio-continuum (Jewitt and Matthews, 1997) $\dot{M}$ values for Hyakutake and would be consistent with the proposal by Harris et al. (1997) that the evaporation of large icy grains produced Hyakutake's spherical gas coma. Finally, one could underestimate the large-grain $\dot{M}$ if the grains are actually more porous than assumed in the calculations, as was pointed out by Harmon et al. (1997) in the context of Hyakutake.

While there remains some uncertainty regarding precisely what fraction of a comet's mass loss is in the form of large grains, it is clear from the radar observations that some comets emit such grains at ~ton/s rates which are within an order of magnitude of their gas and dust production rates. Hence, large grains are not only an important component of the nucleus mass loss, but may also (if evaporating) be a major secondary source of coma gas.

5. Future observations

The full scientific potential of comet radar observations has yet to be fulfilled. The obvious next step is to make delay-resolved measurements using modulated transmissions. This is particularly important for studying comet nuclei. Even a simple echo-versus-delay profile would give a more direct nucleus size estimate than has been available in the past (short of spacecraft imaging). Such a size estimate could then be used to make a more reliable determination of the nucleus' radar albedo (and, hence, surface density). A reliable size would also be a useful constraint for modeling non-radar observations; for example, it could be used to estimate infrared and radio-continuum temperatures for the nucleus surface.

Some close-approaching comets may give sufficiently strong echoes to yield decent delay-Doppler images similar to those that have been obtained for NEAs. From such images one could determine a nucleus' size, shape and (perhaps) rotation. Given sufficient resolution one might even discern surface features such as craters and vents. The best of the NEA delay-Doppler images are those obtained for 4179 Toutatis from Goldstone and Arecibo observations in 1992 (Ostro et al., 1995) and Goldstone observations in 1996 (Ostro et al., 1999). Images with resolutions down to 20 m were obtained when this Hyakutake-size asteroid was at a distance of 0.024 to 0.075 AU. Arecibo images of an even smaller (~1 km) asteroid, 4769 Castalia, though of much coarser resolution, were sufficient to determine this object's size, shape, and rotation at a distance of 0.05 AU (Ostro et al., 1990; Hudson and Ostro, 1994). The Arecibo upgrade increases the S-band radar's sensitivity by an order of magnitude, which effectively increases its distance reach by nearly a factor of two. Hence, even when one takes into account the lower radar albedo of comets, it should be possible to obtain useful radar images for comet nuclei passing within about 0.1 AU of Earth.

Further observations are also needed to better understand grain-coma echoes. Here also, obtaining delay-resolved observations or delay-Doppler images would be a significant advance. The added delay dimension could help to separate the spatial and velocity effects that complicate interpretation of Doppler spectra, provide a more direct measure of halo size (and possible grain evaporation or fragmentation), and better determine jet/fan directions. While delay-Doppler imaging of a coma echo is technically feasible, there are practical problems. First, there are the demanding signal/noise requirements; the relatively

Table 4
Future close apparitions of short-period comets[a]

Comet	Date	Dist. (AU)	Dec. (°)[b]
Encke	17 November 2003	0.261	+38 → +21
Schwassmann–Wachmann 3	12 May 2006	0.082	+32 → +12
Tuttle	2 January 2008	0.252	+42 → +3
d'Arrest	10 August 2008	0.353	−7 → −17[c]
Hartley 2	21 October 2010	0.120	+50 → +27
Honda–Mrkos–Pajdusakova	15 August 2011	0.060	−71 → −24[d]
Encke	17 October 2013	0.478	+40 → +26
Honda–Mrkos–Pajdusakova	11 February 2017	0.089	+6 → +30
Tuttle–Giacobini–Kresak	28 March 2017	0.137	+56 → +60[e]
Giacobini–Zinner	11 September 2018	0.385	+41 → +24
Swift–Gehrels	28 October 2018	0.445	+36 → +37
Wirtanen	16 December 2018	0.075	+3 → +39

[a] Comets passing within 0.5 AU through year 2020.
[b] Declination within 5 days of perigee; the Arecibo declination range is −1° to +38°.
[c] In Arecibo's declination range until 27 July (0.37 AU).
[d] In Arecibo's declination range after 29 August (0.22 AU).
[e] In Arecibo's declination range until 10 March (0.17 AU).

low spectral density implied by the broadband nature of the echo, combined with time slicing of the echo for delay-resolution, requires that the comet be an extremely close approacher (like IAA) with a strong coma echo. Second, the coma observations require a technique different from that used for the nucleus observations; a coded-long-pulse transmission with a long baud (pulse) length would be needed to recover the deep, overspread coma echo, whereas nucleus imaging would use a normal (repeating-code) transmission with a short baud. Finally, interpretation of delay-Doppler images of a coma echo would be much less straightforward than, say, delay-Doppler reflectivity mapping of a rotating spherical planet. An alternative to delay-Doppler imaging is interferometric imaging. Bistatic radar observations, using the Very Large Array (VLA) to make interferometric images of coma echoes from Goldstone 3.5-cm transmissions, can synthesize a beam as small as 0.24 arcsec. This technique, which has been applied successfully to a few asteroids as well as Mercury, Venus, Mars, and Saturn's rings, has significant potential for direct plane-of-sky imaging of the grain comae of close-approaching comets (de Pater et al., 1994, and references therein). Of course, any coma echo detections, be they CW, delay-Doppler, or interferometric, are of considerable interest, especially when they can be compared with other types of observations of cometary activity (infrared, radio, visual). In particular, further comparisons with millimeter and submillimeter continuum observations are important as they may help to resolve some open questions regarding grain properties, such as porosity and electrical conductivity.

We anticipate that radar detections will be attempted at every promising periodic- and 'new'-comet apparition in the next few years. Table 4 shows the closest (<0.5 AU) apparitions of short-period comets for the next two decades. All ten of these comets are potentially detectable at either Arecibo or Goldstone. The Encke apparition in 2003 places it at a slightly better distance than for the 1980 detection. Although this is a poor imaging opportunity, even for the upgraded Arecibo radar, it may be possible to obtain a delay-resolved size estimate for Encke and pin down its still uncertain radar albedo (see Table 3). The 2006 apparition of Schwassmann–Wachmann 3 is the best in terms of range for the next decade. The fact that this comet split into at least four pieces shortly after its 1995 perihelion passage (Crovisier et al., 1996) makes it an interesting, if somewhat uncertain, radar target; optical observations during its next passage in 2001 could provide information on the disposition of the fragments useful in planning possible observations in 2006.

Four of the comets listed as radar candidates in Table 4 are also targets of upcoming spacecraft missions. NASA's planned CONTOUR mission is scheduled to make close flybys of Encke on 12 November 2003, Schwassmann–Wachmann 3 on 18 June 2006, and d'Arrest on 16 August 2008. Each of these flybys would occur within days or weeks of radar observations near perigee (see Table 4). Comet Wirtanen is the rendezvous target of ESA's Rosetta mission in 2011. Although Wirtanen does not make a close pass until 2018, that apparition nominally offers an excellent radar opportunity. We caution, however, that this comet's large nongravitational acceleration (Jorda and Rickman, 1995) could result in a significant departure from the predicted orbit by that time. Comparisons of spacecraft and radar data on any or all of these comets

would be of considerable interest. For example, nucleus sizes derived from spacecraft images could be used to accurately normalize radar albedos.

While it is clear that the short-period comets offer some good radar opportunities in coming years, it is hoped that these will be supplemented by close-approaching 'new' comets similar to IAA, SSF, and Hyakutake. If history is any guide, we might expect the most spectacular results to come from comets as yet undiscovered.

6. Conclusion

Radar observations show comet nuclei to be compact (few-km-size) objects with rough, low-density surfaces. Radar also shows that some comets are emitting large (cm-size) grains in quantities that are comparable with their mass loss in gas and dust, a conclusion which has also been reached from other types of observations. The main limitation in comet radar science has been the fact that all interpretation has had to be based on echo Doppler spectra from CW observations. Therefore, a major goal of future observations is to obtain delay-resolved echoes using modulated transmissions, which would provide direct measurements of nucleus size, accurate radar albedos, and possibly even images. Such observations are now within the capabilities of existing Earth-based radars.

Acknowledgements

We wish to acknowledge the assistance of P. Perillat, A. Crespo, and I. Dauber in the recent Arecibo observations of Comet LINEAR, and of L. A. M. Benner in the Hyakutake observations and analysis. We also wish to recognize several people who contributed to the earlier observational efforts on comets IAA and SSF at Arecibo: A. A. Hine, I. I. Shapiro, G. H. Pettengill, J. F. Chandler, D. K. Yeomans, B. G. Marsden, and R. A. Vélez. Part of this research was conducted at the Jet Propulsion Laboratory, California Institute of Technology, under contract with the National Aeronautics and Space Administration (NASA). The National Astronomy and Ionosphere Center (Arecibo Observatory) is operated by Cornell University under a cooperative agreement with the National Science Foundation and with support from NASA.

References

Altenhoff, W.J., Batrla, W., Huchtmeier, W.K., Schmidt, J., Stumpff, P., Walmsley, M., 1983. Radio observations of Comet 1983 d. Astron. Astrophys. 125, L19–L22.

Altenhoff, W.J., Butler, B., Kreysa, E., Mauersberger, R., McMullin, J., Stumpff, P., Wink, J.E., 1996. Simultaneous radio continuum observations of Comet Hyakutake. Bull. Am. Astron. Soc. 28, 928.

Benner, L.A.M., Ostro, S.J., Giorgini, J.D., Jurgens, R.F., Mitchell, D.L., Rose, R., Rosema, K.D., Slade, M.A., Winkler, R., Yeomans, D.K., 1997. Radar detection of near-Earth asteroids 2062 Aten, 2101 Adonis, 3103 Eger, 4544 Xanthus, and 1992 QN. Icarus 130, 296–312.

Campbell, M.J., Ulrichs, J., 1969. Electrical properties of rocks and their significance for lunar radar observations. J. Geophys. Res. 74, 5867–5881.

Campbell, D.B., Harmon, J.K., Shapiro, I.I., 1989. Radar observations of Comet Halley. Astrophys. J. 338, 1094–1105.

Campbell, D.B., Harmon, J.K., Hine, A.A., Shapiro, I.I., Marsden, B.G., Pettengill, G.H., 1983. Arecibo radar observations of Comets IRAS–Araki–Alcock and Sugano–Saigusa–Fujikawa. Bull. Am. Astron. Soc. 15, 800.

Combi, M.R., 1994. The fragmentation of dust in the innermost comae of comets: possible evidence from ground-based images. Astron. J. 108, 304–312.

Crovisier, J., Bocklée-Morvan, D., Gérard, E., Rauer, H., Biver, N., Colom, P., Jorda, L., 1996. What happened to Comet 83P/Schwassmann–Wachmann 3? . Astron. Astrophys. 310, L17–L20.

de Pater, I., Palmer, P., Mitchell, D.L., Ostro, S.J., Yeomans, D.K., Snyder, L.E., 1994. Radar aperture synthesis observations of asteroids. Icarus 111, 489–502.

de Pater, I., Snyder, L.E., Mehringer, D.M., Wright, M., Veal, J.M., Fernandez, Y.R., Palmer, P., A'Hearn, M.F., 1997. BIMA array observations of Comet Hyakutake: upper limit to the 2.7 mm continuum emission. Planet. Space Sci. 45, 731–734.

Eaton, N., Davies, J.K., Green, S.F., 1984. The anomalous dust tail of Comet P/Tempel 2. Mon. Not. Royal Astron. Soc. 211, 15P–19P.

Fernandez, Y.R., Kundu, A., Lisse, C.M., A'Hearn, M.F., 1997. X-band VLA observations of Comet Hyakutake (C/1996 B2) and implications for nuclear properties. Planet. Space Sci. 45, 735–739.

Fernandez, Y.R., Lisse, C.M., Kundu, A., A'Hearn, M.F., Hoffman, W.F., Dayal, A., 1996. The nucleus of Comet Hyakutake. Bull. Am. Astron. Soc. 28, 1088.

Fulle, M., Mikuz, H., Bosio, S., 1997. Dust environment of Comet Hyakutake 1996B2. Astron. Astrophys. 324, 1197–1205.

Goldstein, R.M., Jurgens, R.F., Sekanina, Z., 1984. A radar study of Comet IRAS–Araki–Alcock 1983 d. Astron. J. 89, 1745–1754.

Hallikainen, M.T., Ulaby, F.T., Abdelrazik, M., 1986. Dielectric properties of snow in the 3 to 37 GHz range. IEEE Trans. Ant. Prop. AP-34, 1329–1339.

Hanner, M.S., 1981. On the detectability of icy grains in the comae of comets. Icarus 47, 342–350.

Hanner, M.S., Newburn, R.L., Spinrad, H., Veeder, G.J., 1987. Comet Sugano–Saigusa–Fujikawa (1983 V) — a small, puzzling comet. Astron. J. 94, 1081–1087.

Hanner, M.S., Aitken, D.K., Knacke, R., McCorkle, S., Roche, P.F., Tokunaga, A.T., 1985. Infrared spectrophotometry of Comet IRAS–Araki–Alcock (1983 d): a bare nucleus revealed? . Icarus 62, 97–109.

Harmon, J.K., Campbell, D.B., Hine, A.A., Shapiro, I.I., Marsden, B.G., 1989. Radar observations of Comet IRAS–Araki–Alcock 1983 d. Astrophys. J. 338, 1071–1093.

Harmon, J.K., Ostro, S.J., Benner, L.A.M., Rosema, K.D., Jurgens, R.F., Winkler, R., Yeomans, D.K., Choate, D., Cormier, R., Giorgini, J.D., Mitchell, D.L., Chodas, P.W., Rose, R., Kelley, D., Slade, M.A., Thomas, M.L., 1997. Radar detection of the nucleus and coma of Comet Hyakutake (C/1996 B2). Science 278, 1921–1924.

Harris, W.M., Combi, M.R., Honeycutt, R.K., Mueller, B.E.A.,

Scherb, F., 1997. Evidence of interacting gas flows and an extended volatile source distribution in the coma of Comet C/1996 B2 (Hyakutake). Science 277, 676–681.

Hudson, R.S., Ostro, S.J., 1994. Shape of asteroid 4769 Castalia (1989 PB) from inversion of radar images. Science 263, 940–943.

Jewitt, D.C., Luu, J., 1992. Submillimeter continuum emission from comets. Icarus 100, 187–196.

Jewitt, D.C., Matthews, H.E., 1997. Submillimeter continuum observations of Comet Hyakutake (1996 B2). Astron. J. 113, 1145–1151.

Jorda, L., Rickman, H., 1995. Comet P/Wirtanen, summary of observational data. Planet. Space Sci. 43, 575–579.

Kamoun, P.G.D., 1983. Radar observations of cometary nuclei. Ph.D. thesis, Mass. Inst. of Tech., Cambridge.

Kamoun, P.G., Pettengill, G.H., Shapiro, I.I., 1982a. Radar detectability of comets. In: Wilkening, L.L. (Ed.), Comets. University of Arizona Press, Tucson, pp. 288–296.

Kamoun, P.G., Campbell, D.B., Ostro, S.J., Pettengill, G.H., Shapiro, I.I., 1982b. Comet Encke: radar detection of nucleus. Science 216, 293–295.

Keller, H.U., Arpigny, C., Barbieri, C., Bonnet, R.M., Cazes, S., Coradini, M., Cosmovici, C.B., Delamere, W.A., Huebner, W.F., Hughes, D.W., Jamar, C., Malaise, D., Reitsema, H.J., Schmidt, H.U., Schmidt, W.K.H., Seige, P., Whipple, F., Wilhelm, K., 1986. First Halley multicolour camera imaging results from Giotto. Nature 321, 320–326.

Luu, J., Jewitt, D., 1990. The nucleus of Comet P/Encke. Icarus 86, 69–81.

Magri, C., Ostro, S.J., Rosema, K.D. Thomas, M.L., Mitchell, D.L., Campbell, D.B., Chandler, J.F., Shapiro, I.I., Giorgini, J.D., Yeomans, D.K., 1998. Mainbelt asteroids: results of Arecibo and Goldstone radar observations of 37 objects during 1980–1995. Submitted to Icarus.

McDonnell, J.A.M., Alexander, W.M., Burton, W.M., Bussoletti, E., Clark, D.H., Grard, R.J.L., Grün, E., Hanner, M.S., Hughes, D.W., Igenbergs, E., Kuczera, H., Lindblad, B.A., Mandeville, J.-C., Minafra, A., Schwehm, G.H., Sekanina, Z., Wallis, M.K., Zarnecki, J.C., Chakaveh, S.C., Evans, G.C., Evans, S.T., Firth, J.G., Littler, A.N., Massonne, L., Olearczyk, R.E., Pankiewicz, G.S., Stevenson, T.J., Turner, R.F., 1986. Dust density and mass distribution near Comet Halley from Giotto observations. Nature 321, 338–341.

Mitchell, D.L., Ostro, S.J., Rosema, K.D., Hudson, R.S., Campbell, D.B., Chandler, J.F., Shapiro, I.I., 1995. Radar observations of asteroids 7 Iris, 9 Metis, 12 Victoria, 216 Kleopatra, and 654 Zelinda. Icarus 118, 105–131.

Ostro, S.J., 1996. NASA/JPL radar telescope observes nucleus of Comet Hyakutake. JPL News Release 9620.

Ostro, S.J., Campbell, D.B., Shapiro, I.I., 1985. Mainbelt asteroids: dual-polarization radar observations. Science 229, 442–446.

Ostro, S.J., Chandler, J.F., Hine, A.A., Rosema, K.D., Shapiro, I.I., Yeomans, D.K., 1990. Radar images of asteroid 1989 PB. Science 248, 1523–1528.

Ostro, S.J., Campbell, D.B., Chandler, J.F., Hine, A.A., Hudson, R.S., Rosema, K.D., Shapiro, I.I., 1991. Asteroid 1986 DA: radar evidence for a metallic composition. Science 252, 1399–1404.

Ostro, S.J., Hudson, R.S., Jurgens, R.F., Rosema, K.D., Campbell, D.B., Yeomans, D.K., Chandler, J.F., Giorgini, J.D., Winkler, R., Rose, R., Howard, S.D., Slade, M.A., Perillat, P., Shapiro, I.I., 1995. Radar images of asteroid 4179 Toutatis. Science 270, 80–83.

Ostro, S.J., Hudson, R.S., Rosema, K.D., Giordini, J.P., Jurgens, R.F., Yeomans, D.K., Chodas, P.W., Winkler, R., Rose, R., Choate, D., Cormier, R.A., Kelley, D., Littlefair, R., Slade, M.A., 1999. Asteroid 4179 Toutatis: 1996 radar observations. Icarus 137, 122–139.

Sarmecanic, J., Fomenkova, M., Jones, B., Lavezzi, T., 1997. Constraints on the nucleus and dust properties from mid-infrared imaging of Comet Hyakutake. Astrophys. J. 483, L69–L72.

Sekanina, Z., 1974. On the nature of the anti-tail of Comet Kahoutek (1973f) I. A working model. Icarus 23, 502–518.

Sekanina, Z., 1988. Nucleus of Comet IRAS–Araki–Alcock (1983 VII). Astron. J. 95, 1876–1894.

Simpson, R.A., 1976. Electromagnetic reflection and transmission at interfaces involving graded dielectrics with applications to planetary radar astronomy. IEEE Trans. Ant. Prop. AP-24, 17–24.

Whipple, F.L., Sekanina, Z., 1979. Comet Encke: procession of the spin axis, nongravitational motion, and sublimation. Astron. J. 84, 1894–1909.